ION PRODUCTION AND RF GENERATION IN THE DARHT-II BEAM DUMP*

M. E. Schulze[ξ], C.A. Ekdahl

Los Alamos National Laboratory, Los Alamos, NM 87545, USA

T.P. Hughes, C. Thoma

Voss Scientific LLC, Albuquerque, NM 87108, USA

Abstract

The DARHT-II accelerator produces a 2-kA, 17-MeV beam in a 1600-ns pulse. After exiting the accelerator, the pulse is sliced into four short pulses by a kicker and quadrupole septum and then transported for several meters to a high Z material target for conversion to x-rays for radiography. The un-kicked beam is diverted to a graphite dump. The interaction of this beam with the dump produces ions that propagate back to the target beamline and affect the beam properties. Coupling of the electron beam and ions to the beam dump vacuum chamber can produce significant amounts of ions and radiofrequency fields (rf) that disrupt the beam transport to the target. This requires a change in the nominal tune to the target. An alternative is to redesign the beam optics in the dump line. The results of a 3D PIC simulation and experimental data are presented along with mitigation techniques to suppress and/or eliminate these effects.

I. INTRODUCTION

The 2-kA, 17-MeV DARHT-II linear induction accelerator [1] is unique in that its beam pulse has a long, 1.6-μs flattop during which the kinetic energy varies by less than +/-2%. Four short pulses are selected out of this long pulse in the downstream transport [2], and these are converted to bremsstrahlung for multi-pulse flash radiography of high explosive driven hydrodynamic experiments. The majority of the beam is transported to the graphite beam dump.

The electron beam interaction with the graphite beam dump produces ions, initially via stimulated desorption and eventually by impact ionization of thermally desorbed neutrals as the beam heats the graphite. The result is space charge limited ion current from the heated graphite dump. The ions propagate upstream confined by the potential well of the electron beam. Oscillations in the ion beam couple to the electron beam. With sufficient ion current, the induced oscillations in the electron beam couple to the resonant modes of the rectangular vacuum chamber producing the observed rf. The rf causes significant disruption of the beam transport to the target. Additionally, the ions are accelerated back to the target beam line by the beam space charge potential. This can occur in the time between kicked pulses if the beam current is large enough. The ions act as a focusing element and change the beam optics to the target.

Section II describes the beamline layout and optics. Section III describes a 3D PIC code simulation with LSP of the desorption process and the interaction of the ion and electron beam. Section IV presents some beam profile images. A 2D envelope model of the beamline using a residual gas to model the ions is compared with the observed beam images. Section V provides a description of the observed rf including a simulation of the coupling of the resonant modes of the rectangular vacuum chamber to an idealized model of the beam. The present method for suppressing the rf which constrains the transport to the target is described. The design of a modification to the beamline that decouples the beam transport to the target from the beam dump is presented.

II. LAYOUT AND OPTICS

Figure 1 shows a schematic layout of the DARHT-II downstream transport that is addressed in this paper. The beam from the accelerator (long pulse region) is focused to a waist in the region upstream of the septum quad using the solenoid just upstream of the kicker. The bias dipole, collocated with the kicker, deflects the beam downward by about 1 to 1.5°. The beam enters the horizontally focusing septum quad and is deflected further downward by a total of about 15°. The dipole completes a 45° bend. The design and function septum dump quadrupole is discussed in Section V.

* Work supported in part by the US Dept of Energy under contract DE-AC52-06NA25396

ξ email: schulz@lanl.gov

Report Documentation Page

Form Approved
OMB No. 0704-0188

1. REPORT DATE	2. REPORT TYPE	3. DATES COVERED
JUN 2013	**N/A**	**-**

4. TITLE AND SUBTITLE
ION Production And Rf Generation In The Darht-Ii Beam Dump

5a. CONTRACT NUMBER
5b. GRANT NUMBER
5c. PROGRAM ELEMENT NUMBER

6. AUTHOR(S)

5d. PROJECT NUMBER
5e. TASK NUMBER
5f. WORK UNIT NUMBER

7. PERFORMING ORGANIZATION NAME(S) AND ADDRESS(ES)
Los Alamos National Laboratory, Los Alamos, NM 87545, USA

8. PERFORMING ORGANIZATION REPORT NUMBER

9. SPONSORING/MONITORING AGENCY NAME(S) AND ADDRESS(ES)

10. SPONSOR/MONITOR'S ACRONYM(S)
11. SPONSOR/MONITOR'S REPORT NUMBER(S)

12. DISTRIBUTION/AVAILABILITY STATEMENT
Approved for public release, distribution unlimited

13. SUPPLEMENTARY NOTES
See also ADM002371. 2013 IEEE Pulsed Power Conference, Digest of Technical Papers 1976-2013, and Abstracts of the 2013 IEEE International Conference on Plasma Science. IEEE International Pulsed Power Conference (19th). Held in San Francisco, CA on 16-21 June 2013., The original document contains color images.

14. ABSTRACT
The DARHT-II accelerator produces a 2-kA, 17-MeV beam in a 1600-ns pulse. After exiting the accelerator, the pulse is sliced into four short pulses by a kicker and quadrupole septum and then transported for several meters to a high Z material target for conversion to x-rays for radiography. The un-kicked beam is diverted to a graphite dump. The interaction of this beam with the dump produces ions that propagate back to the target beamline and affect the beam properties. Coupling of the electron beam and ions to the beam dump vacuum chamber can produce significant amounts of ions and radiofrequency fields (rf) that disrupt the beam transport to the target. This requires a change in the nominal tune to the target. An alternative is to redesign the beam optics in the dump line. The results of a 3D PIC simulation and experimental data are presented along with mitigation techniques to suppress and/or eliminate these effects.

15. SUBJECT TERMS

16. SECURITY CLASSIFICATION OF:			17. LIMITATION OF ABSTRACT	18. NUMBER OF PAGES	19a. NAME OF RESPONSIBLE PERSON
a. REPORT	b. ABSTRACT	c. THIS PAGE			
unclassified	**unclassified**	**unclassified**	**SAR**	**8**	

The kicked beam enters the septum quadrupole on axis and the nominally round beam profile becomes elliptical. The function of the small quadrupoles following the septum quadrupole is to transform this elliptical beam back to a round profile. The purpose of the remaining solenoid is to transport the beam to the final focus solenoid which delivers a tightly focused beam to the target. The imaging station located after this solenoid is used to measure the beam profile. The spacing between the kicked pulses is typically 475 ns. The distance from the beam dump to the septum entrance is 2.2 m. Figure 2 shows measurements of the typical beam current at the cathode, accelerator exit and target.

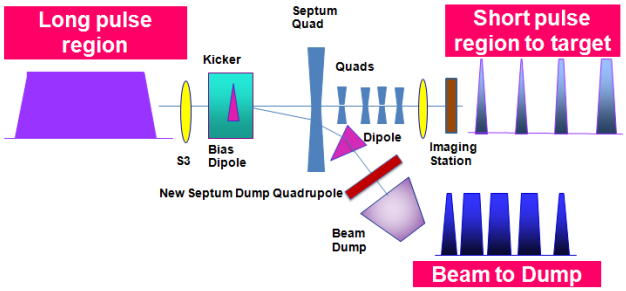

Figure 1. Schematic layout of the downstream transport

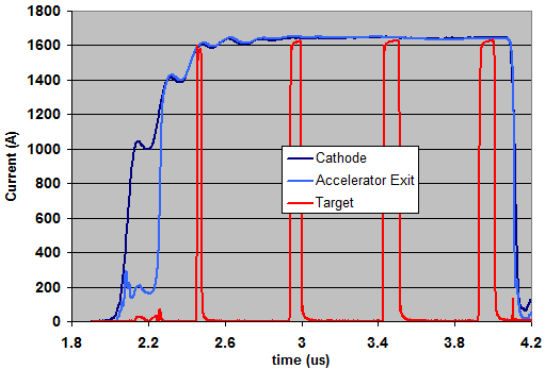

Figure 2. Typical beam current signals at cathode, accelerator exit and target

III. LSP SIMULATION

LSP [3] simulations were performed to model stimulated desorption of ions created at the graphite beam dump by the un-kicked electron beam. The purpose of the simulation was to determine if back-streaming ions might alter the beam transport to the target. Simulations were performed for two cases.

- 7.8 MeV, 950 A and $n_i/n_e=10^{-4}$
- 18.4 MeV, 2 kA and $n_i/n_e=10^{-3}$

The ion yields of 10^{-4} and 10^{-3} correspond to desorption cross sections of 10^{-19} and 10^{-18} cm^2 respectively. The ion species is assumed to be H^+ resulting from impact ionization of H_2O. Although there is no direct measurement of these cross sections, Genoni and Hughes [4] have determined a cross section of 10^{-18} cm^2 for electron impact ionization of H_2O based on an extrapolation from low energy data [5]. Different values used for the ion yields to help bound the problem. Hughes and Davis [6] provide a description of the desorption model.

Since one of the questions of interest was to determine whether the desorbed ions will propagate to the target beamline on a timescale of several hundred ns, it was decided to treat all desorbed ions as H^+ since they will travel much faster than either OH^+ or H_2O^+. The ion velocity can be estimated from the beam potential. The maximum beam potential on axis of a relativistic hard-edged round beam of radius a in a pipe of radius b is given by Eq. (1) [7.]

$$V_{\max}\left[kV\right] = 30I\left[kA\right]\left(1+2\ln\left(b/a\right)\right) \qquad (1)$$

This corresponds to an H+ ion velocity given by Eq. (2).

$$v_{H^+}/c \sim \sqrt{\frac{2eV_{\max}}{938.3}}\,. \qquad (2)$$

Just upstream of the septum quad the beam radius is 1.0 cm and the beam pipe radius is 9.2 cm. The ion velocities are about 0.55 and 0.79 cm/ns for the 7.8 and 18.4 MeV simulations respectively. The ions need to travel about 2.2 m in the 450 ns between pulses or 0.49 cm/ns. This suggests the possibility of ions propagating back to the target beamline between kicked pulses in both cases.

Figures 3-9 show the LSP results simulating the propagation of the ions back to the target beam line at different times for 18.4 MeV and 2.0 kA. The horizontal axis is centered (z=0 cm)at the quad septum. In each of these figures the electron beam is shown in blue and the ions in green. Figure 3 shows the results after 89 ns. The ions are strongly focused as they propagate upstream. Figure 4 shows a periodic focusing of the ions consistent with a frequency in the 1-2 GHz range after 222 ns. Figure 5 shows that ions reach the target beamline after 356 ns. At 445 ns the ions have almost reached the kicker (-100 cm) as shown in Figure 6. Figure 7 is at the same time as Figure 4 showing the electron beam only. The focusing of the electron beam due to space charge neutralization is clearly evident in Figure 7 and the estimated temperature of the graphite dump is 935°K. Figure 8 shows the ions and electrons at the beginning of the kicker pulse after 467 ns. The kicker pulse is simulated by turning off the bias dipole in a 10 ns linear ramp. Figure 9 shows the ions and electrons after the bias dipole has been off for 10 ns. Note that the ions are still in the path of the electron beam.

The results of the LSP simulation show the ions from the 7.8 MeV beam require 576 ns to reach the target beamline. This implies that backstreaming ions will not affect the beam transport to the target due to the nominal 500 ns between kicked pulses. The assumption is that the unconfined ions propagate to the wall of the vacuum chamber during the kicked pulse as suggested by Figure 9. Figure 10 shows a plot of the horizontal and vertical beam envelopes for the fully kicked beam at different

times in the 18.4 MeV simulation. The black trace shows the beam envelope without any ions. The red and blue traces correspond to simulations at 480 and 512 ns respectively. The additional focusing due to space charge neutralization is clearly evident in these traces. The charge neutralization fraction, $f_e=n_i/n_e$, is 0.65%.

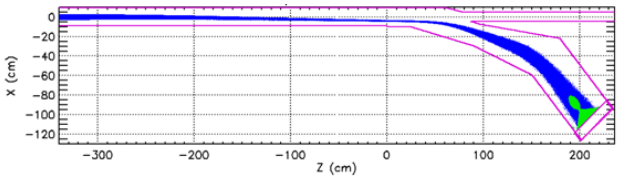

Figure 3. 18.4 MeV – 2.0 kA simulation at 89 ns (Blue electrons) (Green ions)

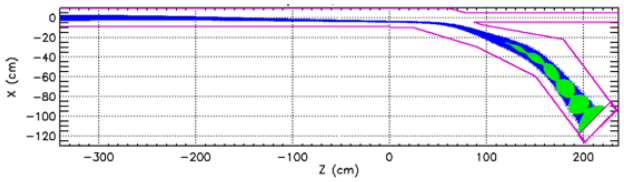

Figure 4. 18.4 MeV – 2.0 kA simulation at 222 ns (Blue electrons) (Green ions)

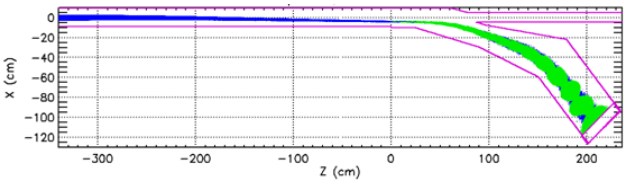

Figure 5. 18.4 MeV – 2.0 kA simulation at 356 ns (Blue electrons) (Green ions)

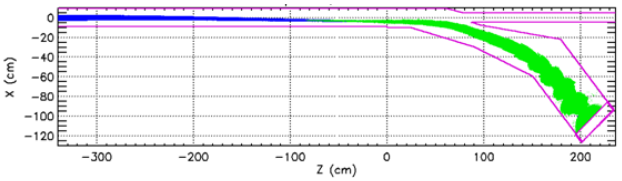

Figure 6. 18.4 MeV – 2.0 kA simulation at 445 ns (Blue electrons) (Green ions)

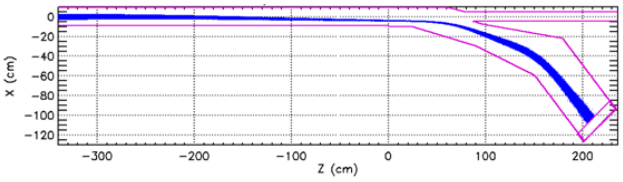

Figure 7. 18.4 MeV–2.0 kA simulation at 445 ns (no ions)

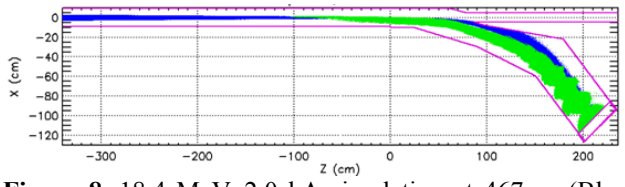

Figure 8. 18.4 MeV–2.0 kA simulation at 467 ns (Blue electrons) (Green ions)

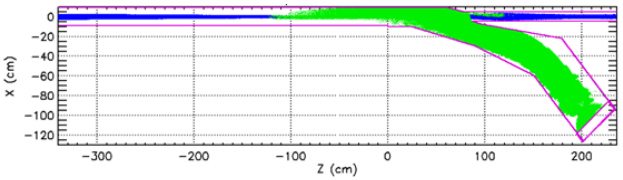

Figure 9. 18.4 MeV–2.0 kA simulation at 489 ns (Blue electrons) (Green ions)

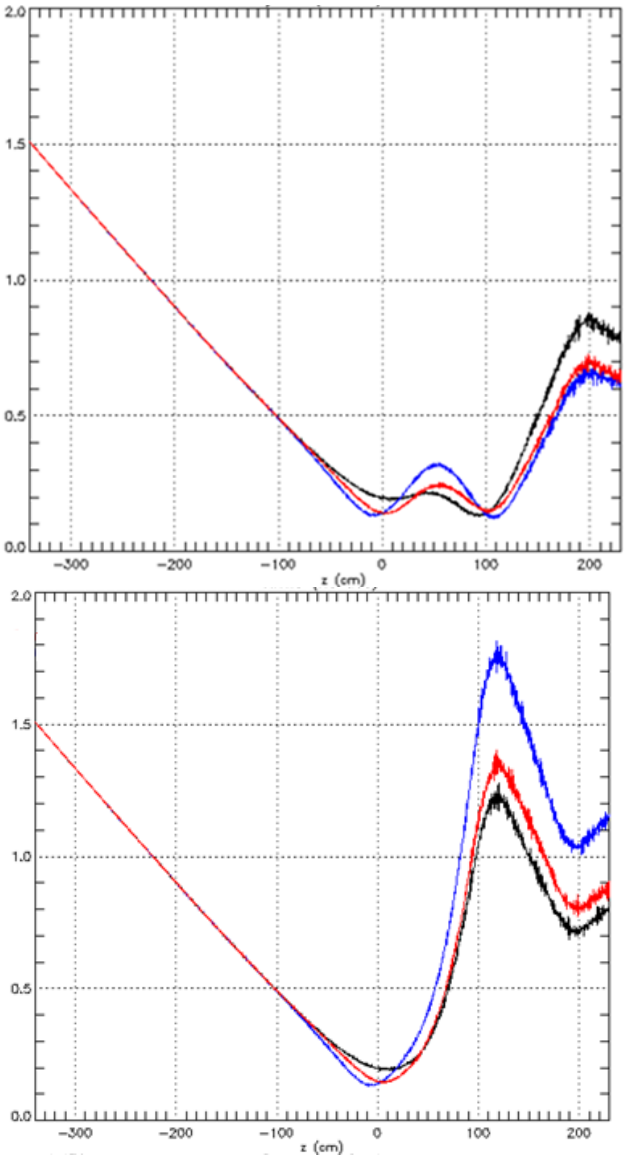

Figure 10. Horizontal (upper) and vertical (lower) beam envelopes in cm at different times for the 18.4 MeV simulation (Black trace no ions) (Red trace 480 ns) (Blue trace 512 ns)

IV. BEAM PROFILE MEASUREMENTS

Beam profile measurements made at the imaging station shown in Figure 1 for two different beam energies and currents for each of the four kicked pulses are shown in Figure 11. Measurements made at 8.0 MeV and 1.0 kA with a pulse spacing of 400 ns are shown in the upper row. Measurements made at 16.5 MeV and 1.88 kA with a pulse spacing of 450 ns are shown in the lower row. The horizontal and vertical FWHM are shown below each image.

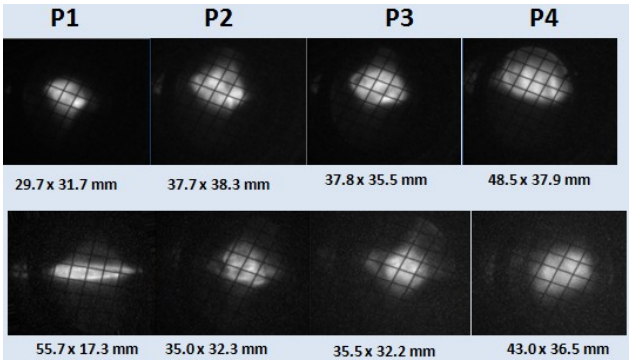

Figure 11. Beam profile measurements for P1-P4 for 8.0 MeV and 1.0 kA (upper) and 16.5 MeV and 1.88 kA (lower)

The measurements at 8.0 MeV show a similar shape for all four pulses. The increase in the spot size from P1 to P4 is attributed to the increase in energy of about 4% from P1 to P4. In addition, the measured spot sizes are in agreement with the predicted spot sizes based on measurements at the accelerator exit. Although this can be considered a null result, it is consistent with the LSP results from the previous section.

The P1 pulse is significantly different than P2-P4 for the measurements at 16.5 MeV. To better understand and possibly explain this difference 2D beam envelope simulations were made using LAMDA [8]. Using the magnet setting and measured fields if the magnets, the beam emittance, radius and divergence at the accelerator exit were fit to obtain the measured P1 beam profile. A residual gas located between the kicker and septum is introduced to simulate the effect of the ions. It is assumed that the small amount of beam prior to P1 (~200 ns) as shown in Figure 2 will not produce ions that reach the target beamline. This is consistent with the simulation in Figure 4.

The process by which the beam produces ions in a residual gas is time dependant and LAMDA is designed to solve the envelope equation for time dependent beam distributions. The beam-induced ionization model in LAMDA calculates a time dependent charge neutralization fraction based on the gas pressure, p, time, t, and gas ionization constant, α, as given by Eq. (3).

$$f_e = \frac{p(torr)t(ns)}{\alpha} \tag{3}$$

Figure 12 shows the results of the LAMDA calculation for a charge neutralization fraction of 0.62%. The gas was present between -112 cm to +52 cm. The imaging station is located at z=750 cm. The simulations agree with the measured beam sizes to better than 2% for P1, P2 and P3. The predicted P4 spot size is about 10% smaller than the measured value in both planes.

A comparison of the LAMDA simulation results with the LSP simulation shows that the charge neutralization fractions are essentially the same. The distance over which the residual gas was introduced is in good agreement with the region over which ions are present in Figure 9. These results indicate that the amount of backstreaming ions used in the LSP simulation and the ion velocity are consistent with the measurements.

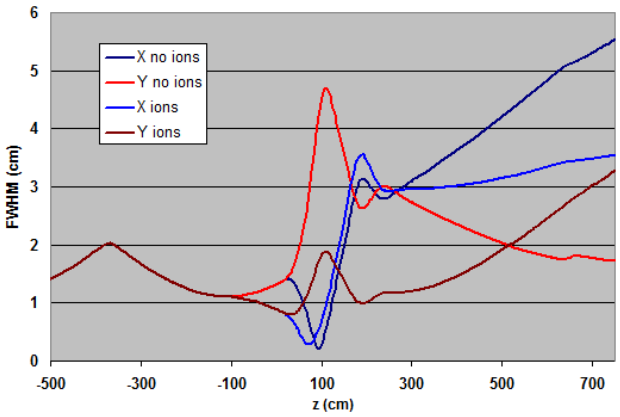

Figure 12. LAMDA simulation with and without ionizing gas

V. RF ISSUES AND MITIGATION

A. The Problem with RF

RF radiation in the 1-2 GHz range has been observed on many devices in the DARHT-II downstream transport. These include high bandwidth beam position monitors (BPMs) and the kicker electrodes. Figure 13 shows an example of rf on a kicker electrode with a single kicker pulse. The amplitude of the kicker pulse is about 15 kV. The amplitude of the rf exponentially increases until the beam is turned off. Figure 14 shows another example of rf with four kicker pulses. The amplitude of the third and fourth kicker pulses is reduced and the voltage is oscillating at the rf frequency. The beamline between the kicker and the target includes a 3 m section with a cutoff frequency of 1.79 GHz. BPMs in the target region show signal with rf structure at 1.26 and 1.61 GHz. This demonstrates the oscillation is present on the beam pulse. Figure 15 shows the frequency spectrum for the kicker waveform in Figure 14. The typical quality factor or Q value is about 1000.

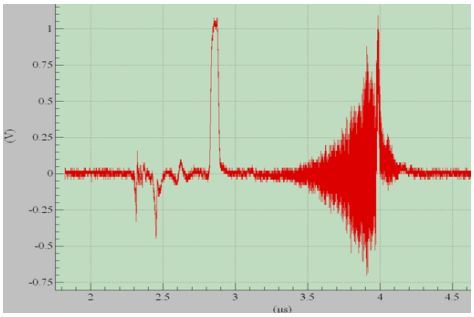

Figure 13. RF observed on a kicker electrode

The oscillation on the kicker pulse causes significant distortion of the focused spot size on target as shown in Figure 16. The image on the right in Figure 16 shows the P4 spot size without rf (FWHM = 0.9mm) and with rf (FWHM~ 2.6 mm). In addition to the distortion of the spot size, the amplitude of the P4 kicked pulse is about 20% less as shown in Figure 17. Figure 18 shows the corresponding frequency spectrum for the kicker waveform in Figure 17. Note that the frequency spectra in Figures 15 and 18 show resonances at different frequencies. For comparison, Figures 19 and 20 show the kicker waveform and corresponding frequency spectrum for a shot without rf.

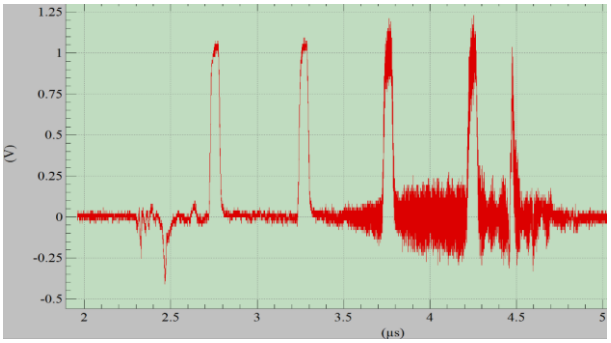

Figure 14. RF observed on a kicker electrode

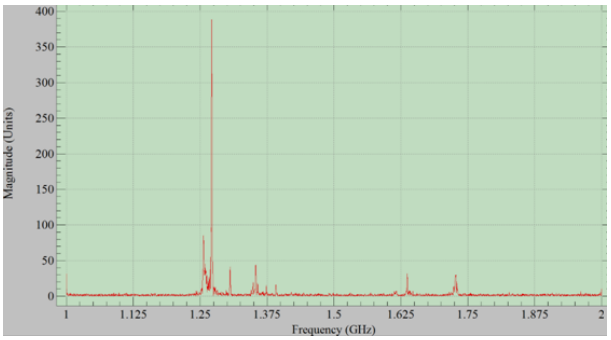

Figure 15. Frequency spectrum of Figure 14 waveform

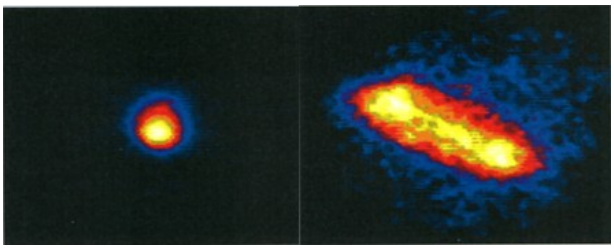

Figure 16. P4 spot size on target without rf on left and with a small amount of rf on right

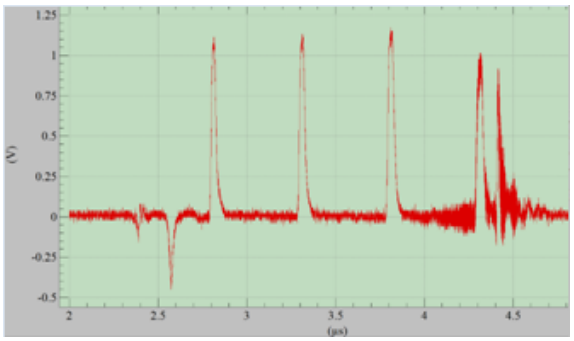

Figure 17. Kicker waveform for shot with rf in Figure 16

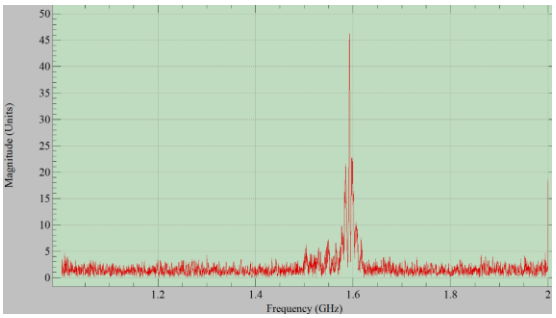

Figure 18. Frequency spectrum for the kicker waveform in Figure 17

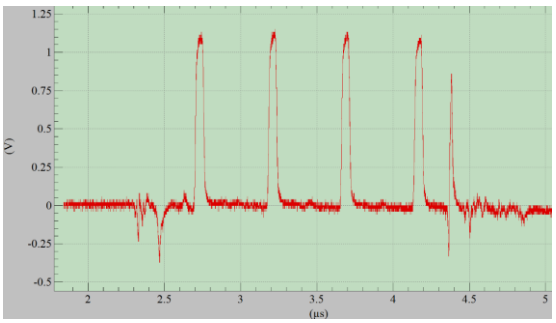

Figure 19. Kicker waveform for shot without rf

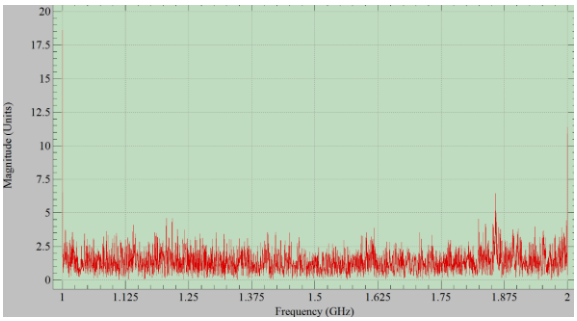

Figure 20. Frequency spectrum for the kicker waveform in Figure 17

B. HFSS Simulation

In order to better understand the observed rf in the dump region, electromagnetic field simulations were performed using HFSS [9, 10] to simulate the interaction of an electron beam with the vacuum chamber between the kicker and the dump. The beam was modeled as a current source on the surface of a curved cylinder of 3.0" diameter along the calculated beam trajectory. A solid model of the vacuum chamber was imported into HFSS. The dump vacuum chamber is about 10 cm wide with a height increasing from about 15 cm to 35 cm as measured perpendicular to the beam trajectory. The field patterns were calculated for frequencies between 1 and 2 GHz in 5 MHz steps. Figures 21 and 22 show the calculated field patterns at 1.26 and 1.61 GHz respectively. These correspond to the dominant frequencies seen in Figures 15 and 18. There are many other frequencies that can be excited by the beam. Figure 23 shows the relative strength of all frequencies excited by the beam in the dump vacuum chamber as calculated in the HFSS simulation. The frequency spectrum in Figure 23 is based on a table with 10 MHz steps and does not show the high Q response seen in Figures 15 and 18. Figure 24 shows another frequency spectrum measured at the kicker electrodes with much of the same structure seen in the HFSS simulation. The different frequency spectra in Figures 15, 18 and 24 are believed to be due to small changes in the beam size and trajectory. Note that the peak below 1.1 GHz is below the cutoff frequency of the beam pipe between the dump and the kicker.

The HFSS simulations demonstrate that the observed frequency structure is consistent with beam interactions with the dump vacuum chamber. The oscillations in the backstreaming ion envelope as seen in Figure 4 will induce oscillations in the electron beam that will resonate with the dump vacuum chamber.

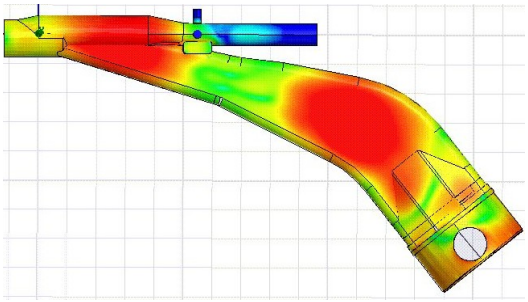

Figure 21. Calculated field pattern at 1.26 GHz

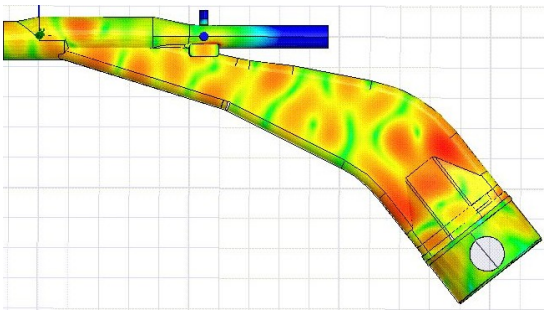

Figure 22. Calculated field pattern at 1.61 GHz

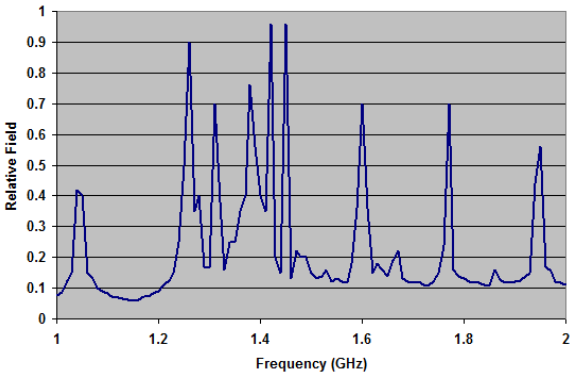

Figure 23. HFSS calculation of frequency spectrum

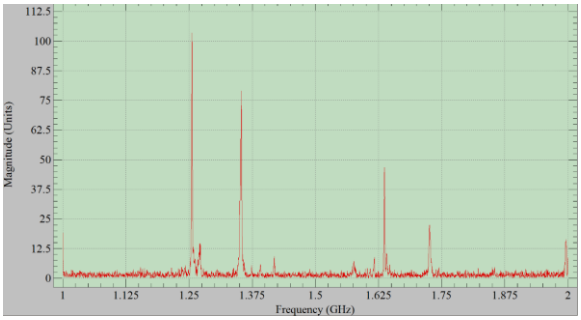

Figure 24. Frequency spectrum with similar structure to HFSS simulation

C. RF Mitigation

The rf was first observed during operations at 8.0 MeV and 1.0 kA. At this time, the rf was easily suppressed by small steering changes of the beam trajectory between the kicker and the dump. Very little effort was made to understand the phenomena. During initial beam

operations at 18.4 MeV and 2.1 kA, rf was also observed. During the process of tuning the downstream transport at this energy and current, the rf was readily suppressed.

During tuning of the downstream transport at 17.0 MeV and 1.9 kA, the rf persisted and could not be suppressed. Figure 13 shows a typical rf signal on the kicker electrode. The key observation was that the rf never appeared early in the beam pulse. This suggested an interaction with the beam dump. An experiment was performed in which the beam size on the beam dump was deliberately changed to see if this affected the rf. The field in the solenoid magnet (S3) just upstream of the kicker in Figure 1 was increased corresponding to an increase in the beam size on the dump. As the field was increased the onset of the rf signal moved later in time. Figure 25 shows the rf on the kicker electrode for four different solenoid currents demonstrating that increasing the beam size on the dump will suppress the rf. Note that the pulse length in the traces shown in Figure 25 is about 500 ns shorter that the full pulse length and a solenoid current of 72 A is generally required to suppress rf at full pulse length.

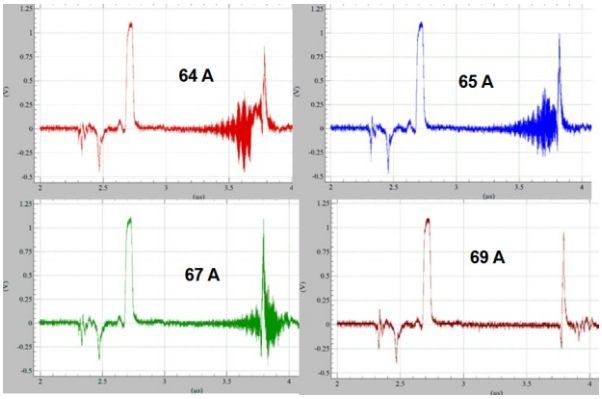

Figure 25. Kicker electrode signal for different solenoid focusing strengths

Figure 26 shows a BPM signal for the shots shown in Figure 25. The BPM is located 35 cm upstream of the surface of the graphite dump. The enhanced current signal on the traces with rf (64, 65 and 67 A) is associated with the presence of rf and is not believed to be backstreaming ions. This clearly shows the onset of the rf is later in time as the beam size is increased. The actual ion current is believed to be at most 1-2 A for space charge limited emission. The BPM is an inductive pickup which measures dB/dt.

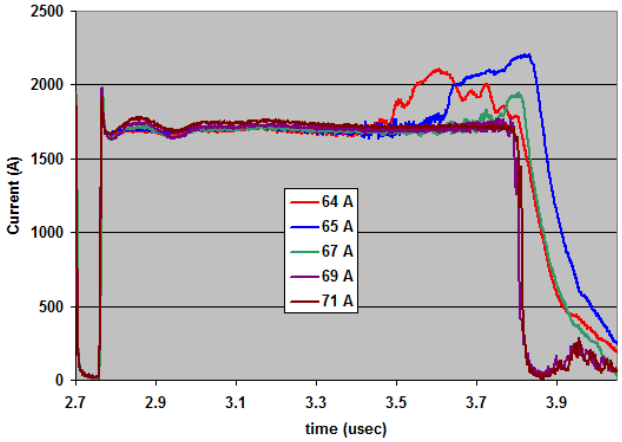

Figure 26. BPM signal for same shots in Figure 25

Figures 25 and 26 show how the rf is suppressed by increasing S3. Figure 27 shows beam images of P1, P2 and P3 taken with a tune similar to the 16.5 MeV tune used to acquire the images in Figure 11 for 16.5 MeV. The beam size for P2 and P3 is now essentially the same as that for P1 and the P1 spot size is the same as that presented in Figure 11. This indicated that the affect of the backstreaming ions is also mitigated by increasing the beam size on the dump. No comparable P4 images were taken at this time.

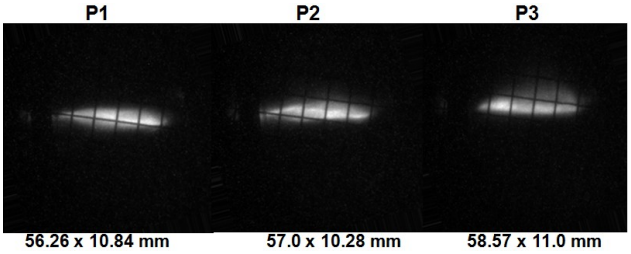

Figure 27: Beam images with S3 increased to suppress rf

One consequence of increasing the solenoid field to suppress the rf is that the beam size of the kicked beam is also increased and beam losses of 10% have been observed. Other methods to suppress the rf such as lining the vacuum chamber with ferrite have been examined. The ferrite will dampen the rf but does not suppress the ions. A dump quadrupole has been designed to decouple the tune to the dump from the tune to the target. The dump quadrupole would be located at the location of the BPM as shown schematically in Figure 1.

The dump quadrupole is shown in Figure 28. The dump quadrupole will focus vertically and transport a larger and rounder beam to the dump. The shape of the poles is designed to fit around the dump vacuum chamber and the pole tips have cutouts to fit around the existing BPM feedthroughs. These introduce significant aberrations but the main purpose of the dump quadrupole to increase the beam size on the dump is accomplished. Figure 29 shows the spot size on the dump with and without the proposed dump quadrupole as a function of

the S3 current for nominal beam conditions. The nominal quadrupole field in the dump quadrupole is 400 Gauss/cm. At this gradient, the dump quadrupole produces beam sizes that are larger than those achieved using S3 at the nominal operating current of 72A required to suppress rf. The dump quadrupole eliminates the constraints in the S3 current and decouples the tune to the target from the tune to the dump.

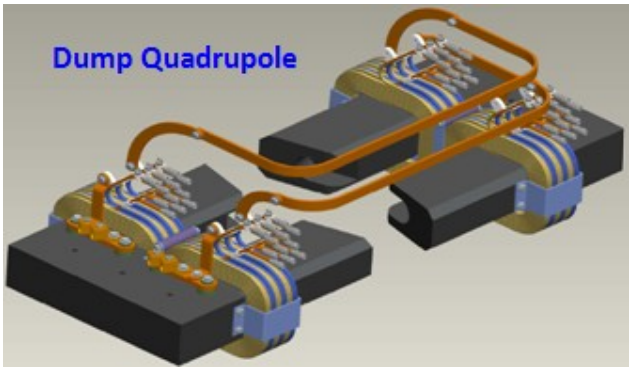

Figure 28. Dump quadrupole

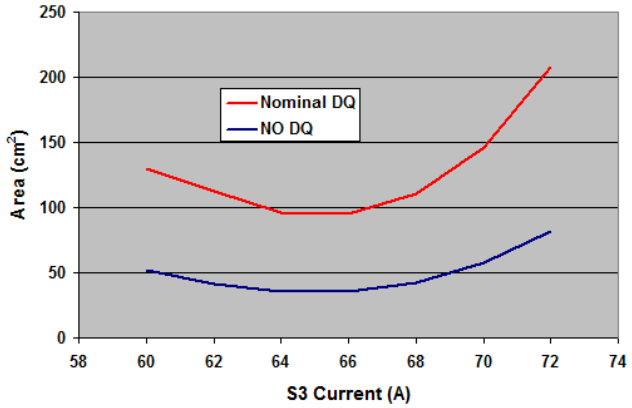

Figure 29. Beam size on dump with and without the proposed dump quadrupole (DQ)

VI. SUMMARY

The presence of ions and rf in the DARHT-II dump region has been extensively studied. Experimental measurements and simulations have been made to understand the observed phenomena. The simulations and measurements show very good agreement.

The problems associated with ions and rf have been mitigated by increasing the beam size at the dump. This accomplishes two goals. The increased beam size reduces the beam heating and delays the onset of the transition from stimulated desorption to space charge limited emission. The increased beam size also significantly reduces the space charge potential of the electron beam resulting is reduced velocities of the backstreaming ions (see Eq. 1 and Eq. 2).

The present approach to increase the beam size on the dump using S3 significantly constrains the beam tune to the target. An engineering solution has been developed using an independent magnet (dump quadrupole) located in the dump beamline. This magnet decouples the beam optics tune to the dump from the tune to the target.

VII. ACKNOWLEDGEMENTS

The authors would like to thank all individuals and sponsors who have participated in the design and operation of the DARHT-II accelerator.

VIII. REFERENCES

[1] Carl Ekdahl, et al., "Electron beam dynamics in the long-pulse, high-current DARHT-II linear induction accelerator", in Proc. 2009 Particle Accelerator Conf., pp. 3080-3084 (May 2009).
[2] Martin Schulze, et al., "Commissioning the DARHTII Accelerator Downstream Transport and Target", in Proc. 2008 Linear Accel. Conf., pp. 427-429 (Sept. 2008).
[3] LSP is a software product of ATK Mission Research.
[4] T. C. Genoni and T. P. Hughes, "Ion-hose instability in a long-pulse linear induction accelerator", Phys. Rev. ST Accel. Beams, 6, 030401, 2003.
[5] M.V.V S. Rao, I. Iga, and S.K. Srivastava, "Ionization cross-sections for the production of positive ions from H2O by electron impact", *J. Geophys. Res.*, 100:26421, 1995.
[6] T. P. Hughes and H. Davis, "Effect of Stimulated and Thermal Desorption ain DARHT-2", in Proc. 2003 Particle Accel. Conf., pp. 120-122 (2003).
[7] M. Reiser, "Theory and Design of Charged Particle Beams", John Wiley and Sons, New York, 1994.
[8] T.P. Hughes, et al., "LAMDA User's Manual and Reference", Voss Scientific Technical Report VSL-0707, April 2007.
[9] HFSS is a product of ANSYS, Inc.
[10] Jim Potter (JPAW), private communication